Catena 237 (2024) 107777

Contents lists available at ScienceDirect

Catena

journal homepage: www.elsevier.com/locate/catena

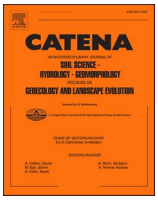

Plant- and microbial-mediated soil organic carbon accumulation in *Spartina alterniflora* salt marshes

Qihang Liao [a,b,c], Feng Yuan [a,b], Qinya Fan [a,b,c], Hongyu Chen [a,b,c], Yameng Wang [a,b], Chuchu Zhang [a,b], Chao Lu [d], Penghua Qiu [e], Chenglong Wang [a,b,*], Xinqing Zou [a,b,c,**]

[a] School of Geographic and Oceanographic Sciences, Nanjing University, Nanjing 210023, China
[b] Ministry of Education Key Laboratory for Coast and Island Development, Nanjing University, Nanjing 210023, China
[c] Collaborative Innovation Center of South China Sea Studies, Nanjing University, Nanjing 210023, China
[d] Institute of Agricultural Resources and Environment, Jiangsu Academy of Agricultural Sciences, Nanjing 210014, China
[e] College of Geography and Tourism, Hainan Normal University, Haikou 571158, China

ARTICLE INFO

Keywords:
Coastal wetland
Chemical stability
Plant- and microbial-derived carbon
Spartina alterniflora invasion
Soil organic carbon
Tide

ABSTRACT

Coastal wetlands play a crucial role in the global carbon (C) cycle; however, they have been affected by the invasive plant *Spartina alterniflora*. The impacts of *S. alterniflora* invasions on soil organic carbon (SOC) source and composition in wetlands are poorly understood compared to SOC stocks. This hinders the accurate estimation of blue C budgets owing to the long-term effects of *S. alterniflora* invasions. Here, a space-for-time substitution method was applied to investigate SOC accumulation in invasive 5-, 10-, 15-, 18-, and 21-year-old *S. alterniflora* communities. This was compared with bare flat in the topsoil (0–10 cm) and subsoil (30–60 cm) of coastal wetlands. Biomarkers (lignin phenols and amino sugars) and Fourier transform infrared spectroscopy were used to describe the accumulation patterns of plant- and microbial-derived C across varying *S. alterniflora* invasion times, as well as associated stabilization mechanisms. Plant-derived C dominated the SOC content compared to microbial-derived C during *S. alterniflora* invasions, while microbial-derived C played a more critical role in SOC stability than that of plant-derived C. At both soil depths, microbial-derived C gradually increased with increasing invasion time, whereas plant-derived C initially increased and then decreased, consistent with changes in SOC content. The variation in inundation conditions, influenced by tides, emerged as a significant factor affecting the accumulation of plant- and microbial-derived C, as well as SOC stability. Decreased inundation frequency and increased oxygen exposure, driven by tides, may lead to a rapid rise in SOC mineralization and the enrichment of microbial-derived C at the expense of plant-derived C. Consequently, this process improved SOC stability. These findings hold substantial implications for potential C loss resulting from the long-term impacts of *S. alterniflora* invasions. Furthermore, they may help predict the long-term effects of *S. alterniflora* invasions on blue C budgets within the context of global change scenarios.

1. Introduction

Coastal wetlands possess a high carbon (C) sequestration capacity, commonly referred to "blue carbon", which plays a crucial role in mitigating global climate change (Wang et al., 2021). Despite covering < 0.1 % of the global surface area, these wetlands accumulate C at a rate 15 times that of terrestrial ecosystems and 50 times that of marine ecosystems, making them capable of offsetting 0.5–1.0 % of current anthropogenic C emissions (Ouyang et al., 2017). However, invasive plants pose a significant threat to coastal wetlands, resulting in considerable uncertainty regarding blue C stocks (Xia et al., 2021).

Spartina alterniflora, a perennial C_4 grass, was introduced to China from the United States in 1979 for coastline protection and soil stabilization (Bernik et al., 2016). Subsequently, *S. alterniflora* has invaded over 40 % of China's coastal wetlands, displacing native C_3 grasses (e.g., *Phragmites australis* and *Suaeda salsa*) and occupying bare flat (BF) areas. This invasion is facilitated by *S. alterniflora's* high photosynthetic rate and its ability to tolerate saline and inundation conditions (Liu et al.,

* Corresponding author.
** Corresponding author at: Xianlin Road 163, Nanjing 210095, China.
E-mail addresses: clwang@nju.edu.cn (C. Wang), zouxq@nju.edu.cn (X. Zou).

https://doi.org/10.1016/j.catena.2023.107777
Received 6 August 2023; Received in revised form 19 November 2023; Accepted 19 December 2023
Available online 29 December 2023

2020). *S. alterniflora* invasions not only threaten the biodiversity of native ecosystems but also affect the process of soil organic C (SOC) accumulation in salt marshes by altering organic litter inputs, rhizodeposition, and sediment capture (Seliskar et al., 2002; Hopkinson et al., 2012). Previous studies have shown that *S. alterniflora* invasions generally promote SOC accumulation owing to its high productivity than that of native salt marshes or BF areas (Yang et al., 2016; Zhang et al., 2021). However, the temporal impacts of *S. alterniflora* invasions on SOC content remain poorly understood. Under the combined effect of elevation and tide, factors such as inundation frequency, soil salinity, clay content, and nutrients vary along the elevation gradient, further affecting the *S. alterniflora* growth (e.g., plant height and biomass) and SOC accumulation across varying invasion times (Deng et al., 2007; Zhang et al., 2010). Additionally, *S. alterniflora* has a proliferative subsurface system, resulting in variations in below-ground biomass and SOC accumulation with soil depth (Li et al., 2020; Liu et al., 2021b). Hence, *S. alterniflora* invasions have diverse impacts on SOC content with increasing invasion time and soil depth (Xia et al., 2021; Xu et al., 2022). However, this inference has not been well explained owing to the varying source, composition, and stability of SOC with increasing invasion time and soil depth remaining poorly understood, limiting our comprehension of the C sequestration process during *S. alterniflora* invasions.

Coastal wetlands are semi-open ecosystems influenced by tides, characterized by high productivity and anoxic conditions that inhibit organic matter decomposition. In this context, abundant plant-derived C (such as lignin phenols) from plant litter and root exudates greatly contributes to SOC (Bernal and Mitsch, 2008). However, recent studies have reported that the "microbial carbon pump" process not only has a critical role in C sequestration in marine and terrestrial ecosystems but also contributes to soil C sequestration in coastal zones (Jiao and Zheng, 2011; Spivak et al., 2019; Liao et al., 2023). As the "engine" of the biogeochemical cycle, microorganisms can use labile C, such as small molecular plant-derived C, to synthesize microbial biomass and then convert it into microbial-derived C (such as amino sugars) via anabolism (Liang et al., 2017; Liu et al., 2021a; Ma et al., 2018). Microbial-derived C can be adsorbed onto mineral surfaces and physically protected in mineral-associated organic matter, resulting in higher stability compared to that of unprocessed plant-derived C stored in particulate organic matter (Liu et al., 2021a; Sokol et al., 2019).

Tidal action plays a pivotal role in SOC turnover and stocks (Schuerch et al., 2019). The thick stems and developed underground rhizomes of *S. alterniflora* can accelerate sedimentation by effectively capturing suspended sediments, thereby increasing elevation and inhibiting tidal action (Davidson et al., 2018; Wang et al., 2022). On the prograding coast, tidal action gradually weakens with increasing *S. alterniflora* invasion time, resulting in changes in microbial activity and SOC sequestration conditions (Wan et al., 2009; Zhu et al., 2019). For instance, decreased inundation frequency and increased soil oxygen exposure lead to increased microbial decomposition of plant residues, and their partial conversion, to more stable microbial necromass via a microbial carbon pump (Liu et al., 2021a). Therefore, the content and stability of SOC are highly dependent on the maintenance of C from plant and microbial sources, which are significantly affected by tides and related environmental factors (Hill and Vargas, 2022; Shao et al., 2022). However, previous studies have mostly focused on the impact of *S. alterniflora* invasions on SOC content in the topsoil of coastal wetlands (Zhang et al., 2010; Davidson et al., 2018), with limited research on the dynamics of plant- and microbial-derived C and their associated stabilization mechanisms in different soil layers.

In this study, a space-for-time substitution method was applied to quantify the response patterns of SOC dynamics to *S. alterniflora* invasions (Liu et al., 2017). Two sets of widely adopted biomarkers (lignin phenols and amino sugars) were selected to trace plant- and microbial-derived C, respectively (Yang et al., 2022). Fourier transform infrared spectroscopy (FTIR) was utilized to evaluate the composition of functional groups and chemical stability of SOC (Calderón et al., 2013; Shao et al., 2019b). We aimed to (1) investigate the accumulation patterns of plant- and microbial-derived C in the topsoil (0–10 cm) and subsoil (30–60 cm) across varying *S. alterniflora* invasion times; and (2) evaluate how *S. alterniflora* invasion influences SOC formation and stability by integrating plant and soil properties as well as tidal conditions.

2. Materials and methods

2.1. Site description and sampling

We conducted this study in the Jiangsu Yancheng Wetland National Nature Reserve buffer region, China (33°21′–33°23′N, 120°42′–120°44′E). The wetland is situated on the middle Jiangsu coast (Fig. 1), which is characterized by continuous seaward advancement, primarily owing to the abundant sediment supply from offshore sand ridges and ancient river deltas (Wang et al., 2012). The study area has a typical monsoon climate, with an annual average temperature of nearly 14 °C and average annual precipitation of about 1000 mm (Yang and Guo, 2018). This region was once a BF area, and *S. alterniflora* was introduced here in the late 1990 s and rapidly expanded to create large areas of *S. alterniflora* salt marshes (Yang, 2019; Yang and Chen, 2021). The growth of *S. alterniflora* is influenced by the complex feedback process of vegetation–tide–sediment, exhibiting co-developmental characteristics with topography and tidal hydrodynamics in its habitat (Fig. 1; Ge et al., 2019; Viles, 2020; Wang et al., 2022). Therefore, the invasion time of *S. alterniflora* exhibits a strong correlation with elevation and tidal hydrodynamics, such as inundation time and frequency (Xie and Gao, 2013; Snedden et al., 2015). Owing to the accelerated sedimentation of *S. alterniflora*, the salt marshes on the middle Jiangsu coast are silted by approximately 4 cm per year, which is equivalent to a 50 m annual advance of the shoreline into the sea (Wang et al., 2012).

A space-for-time substitution method was employed to identify the different *S. alterniflora* invasion times in the sampling area using Landsat images and historical records (Yang and Guo, 2018; Yang, 2019). The chronosequence from seaward to landward included BF, 5-year-old *S. alterniflora* (SA5), 10-year-old SA (SA10), 15-year-old SA (SA15), 18-year-old SA (SA18), and 21-year-old SA (SA21), which were located at distances of 0, 150, 450, 650, 750, and 900 m away from the BF area, respectively (Fig. 1). The BF, SA5, SA10, and SA15 communities were predominantly located in the intertidal zone, which was inundated by semidiurnal tides (average tidal ranges of 3 m) (Xie and Gao., 2013), whereas SA18 and SA21 were primarily within the rarely inundated supralittoral zone. Field sampling was conducted in April 2020. Along three parallel transects (900 m long × 20 m wide), 18 sites were selected across the invasion period. Each transect was 60–80 m apart. At each sampling site, three 1 × 1 m quadrats were randomly established. Depending on the structure of the soil profile and the plant rooting depth, three soil layers (0–10, 10–30, and 30–60 cm) were sampled from each quadrat. To highlight changes at different depths, soil depths of 0–10 and 30–60 cm were selected to represent the topsoil and subsoil, respectively. Following the removal of the organic debris and visible plant roots, three soil replicates were homogeneously mixed to produce one composite sample. The samples were then transported to the laboratory at approximately 0 °C and passed through a 2 mm mesh. Finally, 36 soil samples (6 communities × 3 transects × 2 soil depths) were collected. Each soil sample was divided into two halves: (1) for analysis of soil moisture (SM), clay, microbial biomass C (MBC), and dissolved organic carbon (DOC) (samples stored at 4 °C); (2) salinity, pH, SOC content, SOC chemical stability, total nitrogen (TN) content, lignin phenols, and amino sugars (samples stored at room temperature).

2.2. Analysis of plant properties

In each quadrat (1 × 1 m), the above-ground biomass (AGB) of the plants were collected and delivered to the laboratory. The plant samples

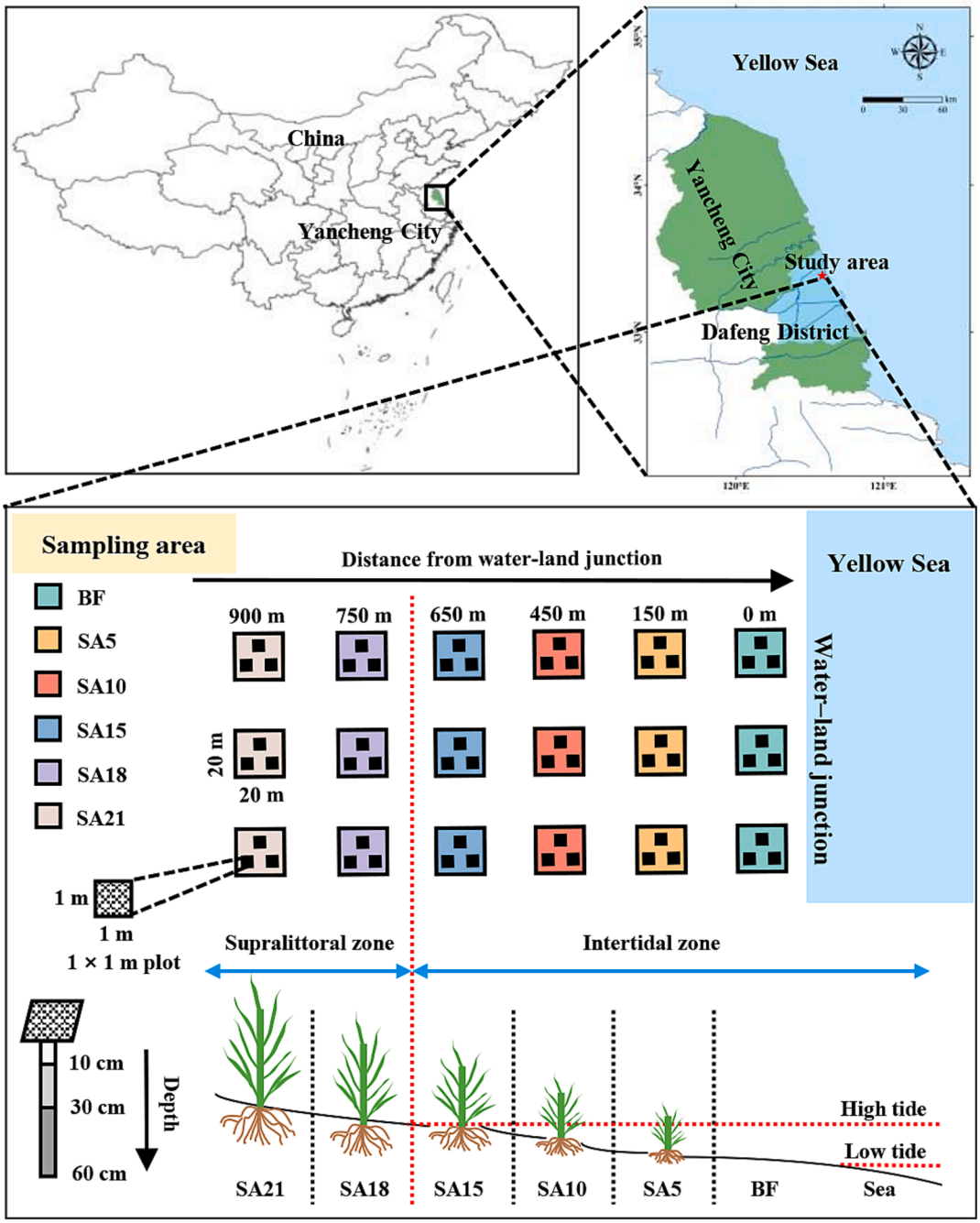

Fig. 1. Location of the sampling sites in the Yancheng Wetland National Nature Reserve buffer region, China. BF: bare flat, SA5: 5-year-old *Spartina alterniflora* (SA), SA10: 10-year-old SA, SA15: 15-year-old SA, SA18: 18-year-old SA, SA21: 21-year-old SA. (For an explanation of the colour reference in this legend, please refer to the Web version of this article.).

were cleaned and dried at 80 °C until a stable weight was obtained. Detailed information regarding the plant properties can be found in Table S1.

2.3. Analysis of soil properties

Soil was oven dried at 105 °C for more than 48 h till the weight was constant to determine the SM. Laser diffraction (Mastersizer 2000, Malvern, UK) was employed to detect the soil texture, with clay, silt, and sand defined as grain sizes of < 2, 2–50, and 50–2000 μm, respectively (Ryzak and Bieganowski, 2011). The electric conductivity method was used to analyze soil salinity. Soil pH was detected by a pH meter in a soil: water ratio of 1:2.5 (w:v). The air-dried soil, sieved to 0.15 mm, was utilized to quantify the SOC and TN contents on a Vario EL III elemental analyzer (Elementar, Germany). The fumigation–extraction approach was used to determine the MBC (Brookes et al., 1985). Soil samples were extracted in MilliQ water at a ratio of 1:2.5 soil solution and shaken for 1 h. The filtered (<0.45 μm) supernatant was then subjected to DOC determination on a multi N/C 3100 automatic analyzer (Analytik, Germany) (Jia et al., 2021).

2.4. FTIR spectroscopy analysis

The SOC chemical stability was measured via FTIR spectroscopy. The KBr pellets were obtained by homogenizing and grinding 2 mg air-dried soil sample (sieved to 0.15 mm) and 200 mg dried KBr. The FTIR spectra

of the soil samples were collected on a Nicolet iN10 infrared spectrometer (Thermo, USA). The measured values were recorded from 4000 to 400 cm^{-1}, with a resolution of 4 cm^{-1} and an average of 64 scans per sample. After subtracting the reflectance related to ambient air, the ratio of the area of a characteristic peak (1630 and 1050 cm^{-1}) to the sum of both selected peaks was calculated as the relative peak areas (rA, %) (Calderón et al., 2013). The ratio between aromatic C groups (active C component; rA1630) and carbohydrates (stable C component; rA1050) was then calculated (rA1630:1050) and used to evaluate SOC chemical stability, following the method of Shao et al., 2019b. A high ratio of rA1630:1050 indicates that the soil has more aromatic nuclei and less aliphatic side chains, and that the soil component has a high degree of condensation and a complex molecular structure (Margenot and Hodson, 2016; Hou et al., 2019).

2.5. Lignin phenols analysis

Soil lignin phenols were determined by alkaline CuO oxidations, combined with gas chromatography, according to the methodology described by Otto et al. (2005). Briefly, 1 g of freeze-dried soil (sieved to 0.15 mm) was mixed with 1 g CuO, 50 mg $Fe(NH_4)_2(SO_4)_2{\cdot}6H_2O$, and 15 mL of 2 M NaOH solution. It was then heated to 170 °C for 3 h in a Teflon bomb. The recovery standards (ethyl vanillin and *trans*-cinnamic acid) were added to the oxidation products and then acidified to pH 1 with 6 M HCl. Cleanert PEP-SPE columns (500 mg, Agela Technologies, USA) were then used to extract the samples. The ethyl acetate eluent was concentrated under N_2 and redissolved in acetonitrile. The obtained samples were derivasized with bis-trimethylsilyl-trifluoroacetamide and 1 % trimethylchlorosilane (BSTFA + 1 %TMCS). The derivasized compounds were loaded on the Thermo Trace 1300 GC instrument DB1 capillary GC column (30 m × 250 μm × 0.25 μm) containing the flame ionization detector.

The quantity of lignin phenols was calculated by adding vanillyl (V)-, syringyl (S)-, and cinnamyl (C)-type phenols. The acid/aldehyde ratios for V and S phenols [$(Ad/Al)_v$ and $(Ad/Al)_s$], and the ratios of C/V and S/V were utilized to estimate the extent of lignin oxidation and microbial alteration (Kögel, 1986). Detailed calculation of the plant-derived C is listed in supplementary methods.

2.6. Determination of amino sugars

Soil microbial-derived C was indicated by amino sugars, including glucosamine (GluN), galactosamine (GalN), and muramic acid (MurN). Soil amino sugars were measured following the procedure of Indorf et al. (2011). Briefly, approximately 1.0 g of freeze-dried soil (sieved to 0.15 mm) was hydrolyzed with 10 mL 6 M HCl at 105 ℃ for 8 h. After cooling, 100 μL myo-inositol (internal standard) was added, and the solution was then filtered. The filtrates were dried using an evaporator (55 ℃) and redissolved in water. The solution was adjusted to pH 6.6–6.8 by KOH neutralization, and the supernatant was dried using an evaporator (55 ℃). Subsequently, the residues were redissolved with 5 mL methanol and then transferred to the vial for drying by N_2 at 45 ℃. Lastly, 100 μL N-methyl glucamine (quantitative standard) and 1 mL deionised water were added into the residues and lyophilized.

Lyophilized residues were dissolved in 300 μL of a derivatization reagent, and the solution was heated at 80 °C for 40 min. Subsequently, 1 mL of acetic anhydride was added to the cooled derivatives and reheated at 80 °C for 30 min. The solution containing 1 mL of 1 M HCl and 1.5 mL dichloromethane was washed three times with 1 mL deionized water to thoroughly remove the residual anhydride. Lastly, 200 μL ethyl acetate-hexane (1:1) was used to redissolve the amino sugar derivatives and analyzed on a Thermo Trace 1300 GC instrument DB1 capillary GC column (30 m × 250 μm × 0.25 μm) containing the flame ionization detector. Detailed calculation of the microbial-derived C is shown in supplementary methods.

2.7. Statistical analysis

All data were checked for normality and homogeneity of variance by the Shapiro–Wilk test and Levene test, respectively. When necessary, log transformation was applied. If a normal distribution was not achieved, then a non-parametric test (Kruskal–Wallis or Mann–Whitney *U* test) was performed. Relationships between different variables were tested using Pearson (normally distributed data) or Spearman correlations. Significant differences of soil properties and biomarkers among the varying invasion times were determined by one-way analysis of variance (ANOVA) with Duncan's test. Differences between soil layers were examined using the paired *t* test. These statistical analyses were performed using SPSS 26.0 for windows (IBM, Corp., USA).

Random forest analysis was utilized to identify the effect of environmental variables on plant- and microbial-derived C. The selected variables included plant properties (AGB), soil biotic factors (MBC), and soil abiotic factors (pH, salinity, clay, SM, SOC, DOC, TN, and C:N). The percentage increase in the mean squared error (MES) was utilized to estimate the relative importance of the environmental variables using the 'randomForest' package in R. With the 'rfPermute' package, the significance of predictors for environmental variables was calculated.

3. Results

3.1. Soil properties

With increasing invasion time of *S. alterniflora*, the SOC content (1.0–7.8 g kg^{-1} soil), TN content (127.4–825.5 mg kg^{-1} soil), clay content (2.3–13.4 %), and salinity (5.8–11.4 g kg^{-1} soil) at both soil depths generally increased first, and then decreased, reaching a peak in the SA10 or SA15 soil (Fig. 2 and Table 1). At both soil depths, the SOC chemical stability (0.07–0.21), DOC (14.4–87.0 mg kg^{-1} soil), and MBC (30.1–221.0 mg kg^{-1} soil) peaked in the SA21 soil (Fig. 2 and Table 1). The soil maintained an alkaline pH at both soil depths, and the pH of BF soil was significantly higher than that of *S. alterniflora* soil ($p = 0.012$; Table 1). The SOC and TN contents of most topsoil were higher than those of the subsoil, whereas the SOC chemical stability in the subsoil was significantly higher than that in the topsoil ($p = 0.001$; Fig. 2 and Table 1). The MBC ($p = 0.009$) and DOC ($p = 0.006$) contents also differed significantly between the topsoil and subsoil (Table 1), with higher values observed in the subsoil, except for the SA15 soil.

3.2. Plant-derived C and its contribution to SOC

The AGB gradually increased with *S. alterniflora* invasion time, ranging from 2851.3 g m^{-2} to 6273.3 g m^{-2} (Table S1). However, the SOC-normalized content of lignin phenols (5.9–50.1 g kg^{-1} SOC), plant-derived C (70.5–3957.6 mg kg^{-1} soil), and the contribution of plant-derived C to SOC (7.4–50.9 %) generally increased initially and then decreased, reaching a peak in the SA15 soil (Fig. 3). The SA21 soil showed the highest ratios of $(Ad/Al)_v$ and $(Ad/Al)_s$ but the lowest ratios of S/V and C/V in *S. alterniflora* areas (Fig. 3). In *S. alterniflora* salt marsh wetlands, the SOC-normalized content of lignin phenols, plant-derived C, and the contribution of plant-derived C to SOC in the topsoil were generally higher than those in the subsoil, whereas the subsoil had higher ratios of $(Ad/Al)_v$ ($p < 0.001$) and $(Ad/Al)_s$ ($p = 0.002$) than the topsoil (Fig. 3).

3.3. Microbial-derived C and its contribution to SOC

In contrast to the plant-derived C, the SOC-normalized content of amino sugars (4.1–30.0 g kg^{-1} SOC), microbial-derived C (27.8–690.8 mg kg^{-1} soil), and the contribution of microbial-derived C to SOC (2.3–21.2 %) generally increased with *S. alterniflora* invasion time at both soil depths. The SA21 soil exhibited significantly higher values for these indicators compared to the other sites ($p < 0.01$; Fig. 3).

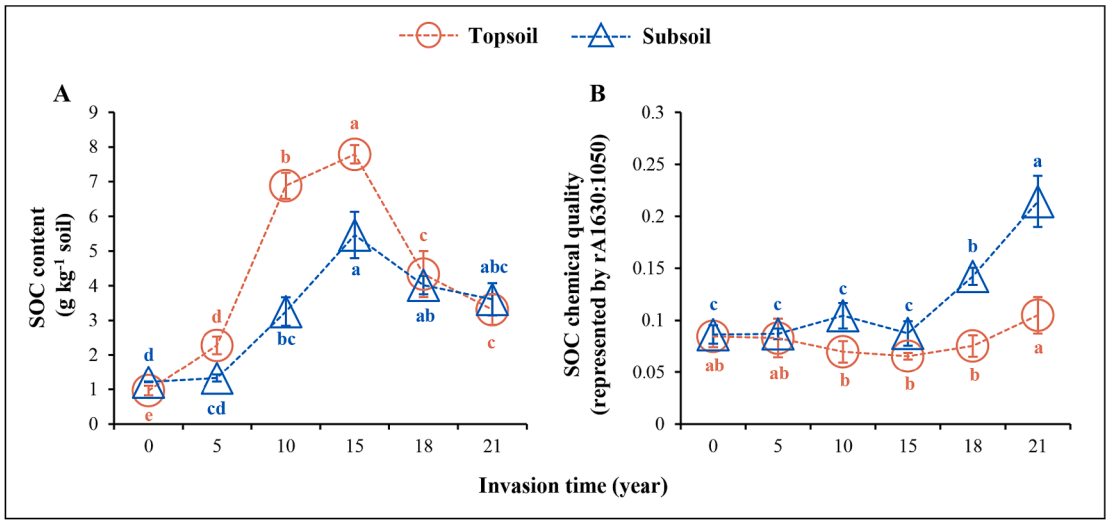

Fig. 2. Soil organic carbon (SOC) content and chemical quality (represented by rA1630:rA1050) across *S. alterniflora* invasion times in the topsoil and subsoil. Error bars represent the standard deviations of triplicate samples. Different superscript letters display the significant differences at $p < 0.05$ across *S. alterniflora* invasion times. (For an explanation of the colour reference in this legend, please refer to the Web version of this article.).

Table 1
Soil properties across *S. alterniflora* invasion times in the topsoil and subsoil.

Soil layer	Soil properties	BF	SA5	SA10	SA15	SA18	SA21	*p* value
Topsoil	SM (%)	23.7 ± 4.8^{a}	45.2 ± 5.2^{a}	45.8 ± 7.1^{a}	41.0 ± 6.2^{a}	44.6 ± 7.7^{a}	35.7 ± 3.3^{a}	> 0.05
	Clay (%)	3.3 ± 0.1^{d}	6.8 ± 0.4^{bc}	13.4 ± 0.6^{a}	11.1 ± 0.9^{b}	6.7 ± 0.5^{bc}	6.3 ± 0.1^{c}	0.007
	DOC (mg kg^{-1} soil)	14.4 ± 1.6^{e}	41.6 ± 6.1^{c}	29.6 ± 3.3^{d}	48.9 ± 6.1^{bc}	53.1 ± 2.9^{b}	69.1 ± 1.9^{a}	< 0.001
	MBC (mg kg^{-1} soil)	30.1 ± 4.1^{d}	37.9 ± 5.7^{d}	46.1 ± 5.8^{d}	81.8 ± 9.4^{b}	65.8 ± 3.5^{c}	107.2 ± 3.4^{a}	0.006
	Salinity (‰)	5.8 ± 0.2^{de}	7.0 ± 0.2^{c}	11.4 ± 0.2^{a}	9.2 ± 0.1^{b}	6.1 ± 0.1^{d}	5.6 ± 0.2^{e}	< 0.001
	pH	7.9 ± 0.1^{a}	7.7 ± 0.1^{b}	7.5 ± 0.2^{cd}	7.7 ± 0.1^{bc}	7.4 ± 0.0^{d}	7.6 ± 0.0^{bc}	< 0.001
	TN (mg kg^{-1} soil)	137.6 ± 11.4^{d}	305.7 ± 10.1^{c}	825.5 ± 29.2^{a}	817.0 ± 21.1^{a}	476.9 ± 89.8^{b}	397.5 ± 71.1^{b}	< 0.001
	C:N	7.0 ± 0.6^{c}	7.4 ± 0.6^{c}	8.3 ± 0.2^{b}	9.5 ± 0.2^{a}	9.1 ± 0.4^{a}	8.4 ± 0.4^{b}	< 0.001
Subsoil	SM (%)	31.2 ± 3.3^{b}	66.7 ± 12.1^{a}	45.5 ± 8.7^{b}	74.6 ± 12.2^{a}	32.9 ± 7.9^{b}	37.7 ± 7.2^{b}	< 0.001
	Clay (%)	2.3 ± 0.3^{d}	4.6 ± 0.2^{c}	8.3 ± 0.1^{b}	12.1 ± 0.9^{a}	8.3 ± 0.5^{b}	8.5 ± 0.4^{b}	0.007
	DOC (mg kg^{-1} soil)	45.0 ± 0.8^{c}	59.7 ± 5.5^{b}	51.3 ± 6.4^{bc}	46.2 ± 4.2^{bc}	86.5 ± 10.9^{a}	86.9 ± 10.8^{a}	< 0.001
	MBC (mg kg^{-1} soil)	68.8 ± 0.8^{bc}	78.4 ± 11.7^{abc}	62.0 ± 7.9^{c}	73.3 ± 6.0^{bc}	$207.2 \pm 2\,5.4^{ab}$	$221.0 \pm 2\,7.9^{a}$	0.020
	Salinity (‰)	5.9 ± 0.3^{e}	9.0 ± 0.2^{c}	10.6 ± 0.4^{b}	11.2 ± 0.1^{a}	7.4 ± 0.1^{d}	7.3 ± 0.1^{d}	0.006
	pH	8.2 ± 0.0^{a}	7.5 ± 0.1^{c}	7.6 ± 0.0^{c}	7.9 ± 0.0^{b}	7.4 ± 0.1^{d}	7.6 ± 0.1^{c}	< 0.001
	TN (mg kg^{-1} soil)	127.4 ± 4.2^{c}	171.0 ± 14.2^{c}	408.6 ± 61.7^{b}	644.8 ± 119.8^{a}	444.6 ± 66.6^{b}	442.1 ± 75.6^{b}	< 0.001
	C:N	9.5 ± 0.2^{a}	7.8 ± 0.5^{b}	8.0 ± 0.4^{ab}	8.5 ± 0.6^{ab}	9.1 ± 0.9^{ab}	8.2 ± 0.4^{ab}	0.046

SM, soil moisture; SOC, soil organic C; DOC, dissolved organic C; TN, total N; C:N, SOC:TN; MBC, microbial biomass C; and AGB, above-ground biomass. The listed values are the mean and standard deviation of the triplicate samples. Different superscript letters in the same row indicate significant differences ($p < 0.05$) across *S. alterniflora* invasion times. BF: bare flat, SA5: 5-year-old *Spartina alterniflora* (SA), SA10: 10-year-old SA, SA15: 15-year-old SA, SA18: 18-year-old SA, and SA21: 21-year-old SA.

Furthermore, the fungal-derived C/bacterial-derived C (F/B) in the SA10 and SA21 soils, at both soil depths, was significantly higher than that in the other sites ($p = 0.002$; Fig. 3). The microbial-derived C in the subsoil was mostly lower than that in the topsoil (Fig. 3). Additionally, compared to the subsoil, the topsoil showed higher bacterial-derived C ($p = 0.001$) and its contribution to SOC ($p < 0.001$), and lower F/B ($p = 0.002$).

3.4. Controls over plant- and microbial-derived C

Random forest models suggested that SOC and TN explained most of the variation of the plant-derived C accumulation at both soil depths ($p < 0.01$; Fig. 4), whereas clay content was the most important factor explaining microbial-derived C ($p < 0.01$). The correlation analysis indicated that plant- and microbial-derived C were positively correlated with clay content at both soil depths ($p < 0.05$; Table S2). Plant-derived C was positively correlated with SOC and TN ($p < 0.01$), whereas microbial-derived C was positively correlated with DOC, MBC, and AGB ($p < 0.05$). Moreover, the contribution of plant-derived C to SOC had a positive correlation with SOC content at both soil depths ($p < 0.01$; Fig. 5), whereas the contribution of microbial-derived C to SOC demonstrated a positive effect on SOC chemical stability ($p < 0.05$).

4. Discussion

4.1. SOC content with S. Alterniflora invasion time

In coastal wetlands located in the land–sea transition zone, periodic tidal action and its controlled vegetation distribution and evolution are the mechanisms that control and maintain the C cycle process and C sink function (Cahoon et al., 2021). Previous studies have indicated that *S. alterniflora* can continuously promote SOC accumulation in China's coastal wetlands, as it does in its native areas (Ouyang and Lee, 2014; Jin et al., 2017). However, the findings from this study showed that the SOC content first increased and then decreased at both soil depths, rather than increasing monotonically, with the highest SOC content in the SA15 soil (Fig. 2). Similarly, a *meta*-analysis also showed that *S. alterniflora* invasions only increased the SOC content on a decadal scale, and then decreased it, which was likely owing to the population degradation of *S. alterniflora* (Xu et al., 2022). Furthermore, microbial-

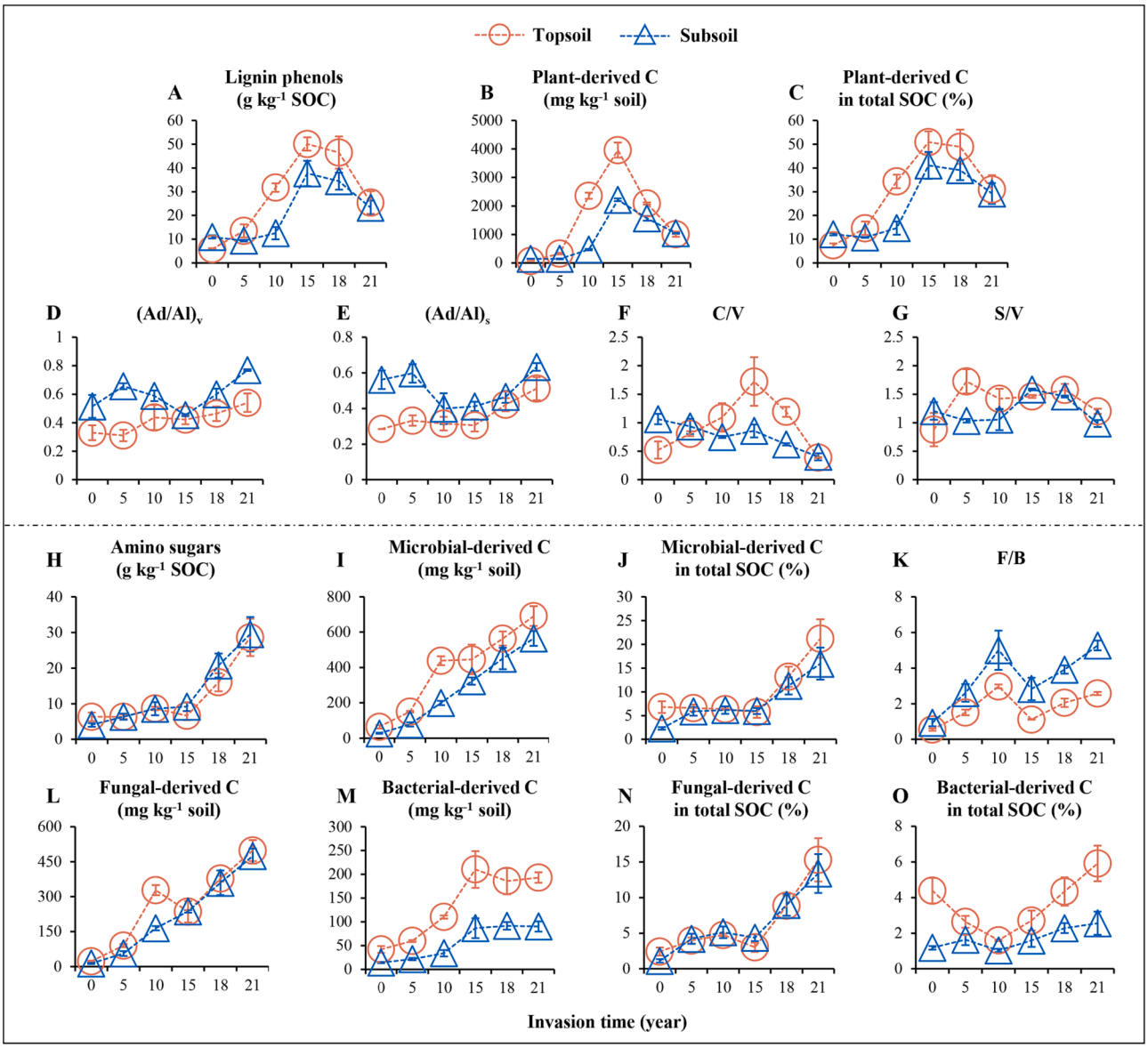

Fig. 3. Content of SOC-normalized lignin phenols (A), content of plant-derived C (B), contribution of plant-derived C to SOC (C), acid-to-aldehyde ratios of syringyl and vanillyl units (Ad/Al; D and E), the ratios of cinnamyl to vanillyl (C/V; F) and syringyl to vanillyl (S/V; G), content of SOC-normalized amino sugars (H), content of microbial-derived C (I), contribution of microbial-derived C to SOC (J), fungal-derived C to bacterial-derived C ratio (F/B; K), fungal- and bacterial-derived C contents (L and M), and fungal- and bacterial-derived C contributions to SOC (N and O) across *S. alterniflora* invasion times in the topsoil and subsoil. Error bars represent the standard deviations of triplicate samples. (For an explanation of the colour reference in this legend, please refer to the Web version of this article.).

mediated C loss increased with invasion time owing to increased greenhouse gas emissions from enhanced microbial decomposition activities (Yuan et al., 2014; Xiang et al., 2015). Consequently, a comprehensive consideration of plant- and microbial-derived C dynamics and their related stabilization mechanisms is required to confirm the long-term impacts of *S. alterniflora* invasions and reveal the underlying mechanisms.

4.2. Accumulation patterns of plant- and microbial-derived C and their contributions to SOC

This study attempted to perform a systematic comparison of soil plant- and microbial-derived C accumulation patterns in different soil layers across *S. alterniflora* invasion times. A conceptual diagram was developed to clarify the mechanisms of plant- and microbial-mediated SOC formation across *S. alterniflora* invasion times on the prograding coastal wetlands (Fig. 6). Topsoil OC in *S. alterniflora* salt marshes was characterized by a high proportion of plant-derived C (7.4–50.9 %) and low proportion of microbial- derived C (5.7–21.2 %) (Fig. 3). The contribution of microbial-derived C to the topsoil OC of *S. alterniflora* salt marshes was lower than that to farmland (55.6 %), grassland (61.8 %), and forest (32.6 %) (<0.25 m) (Liang et al., 2019). Unlike terrestrial ecosystems, coastal wetland ecosystems are affected by the periodic tidal inundation of seawater. *S. alterniflora* can provide abundant plant C to wetland soils owing to its high primary productivity (Liu et al., 2020). The anoxic conditions, caused by inundation, inhibit the decomposition of plant residues by microorganisms and weaken microbial anabolism (Keiluweit et al., 2017; Chen et al., 2021b), resulting in plant-derived C becoming the main component of the wetland SOC pool (Fig. 3).

The distinct sources of SOC across *S. alterniflora* invasion times have significant influences on their stability. Studies have increasingly recognized that plant-derived C has lower stability and persistence than microbial-derived C as it is less physically protected in mineral-associated organic matter (Ma et al., 2018). At both soil depths, plant-

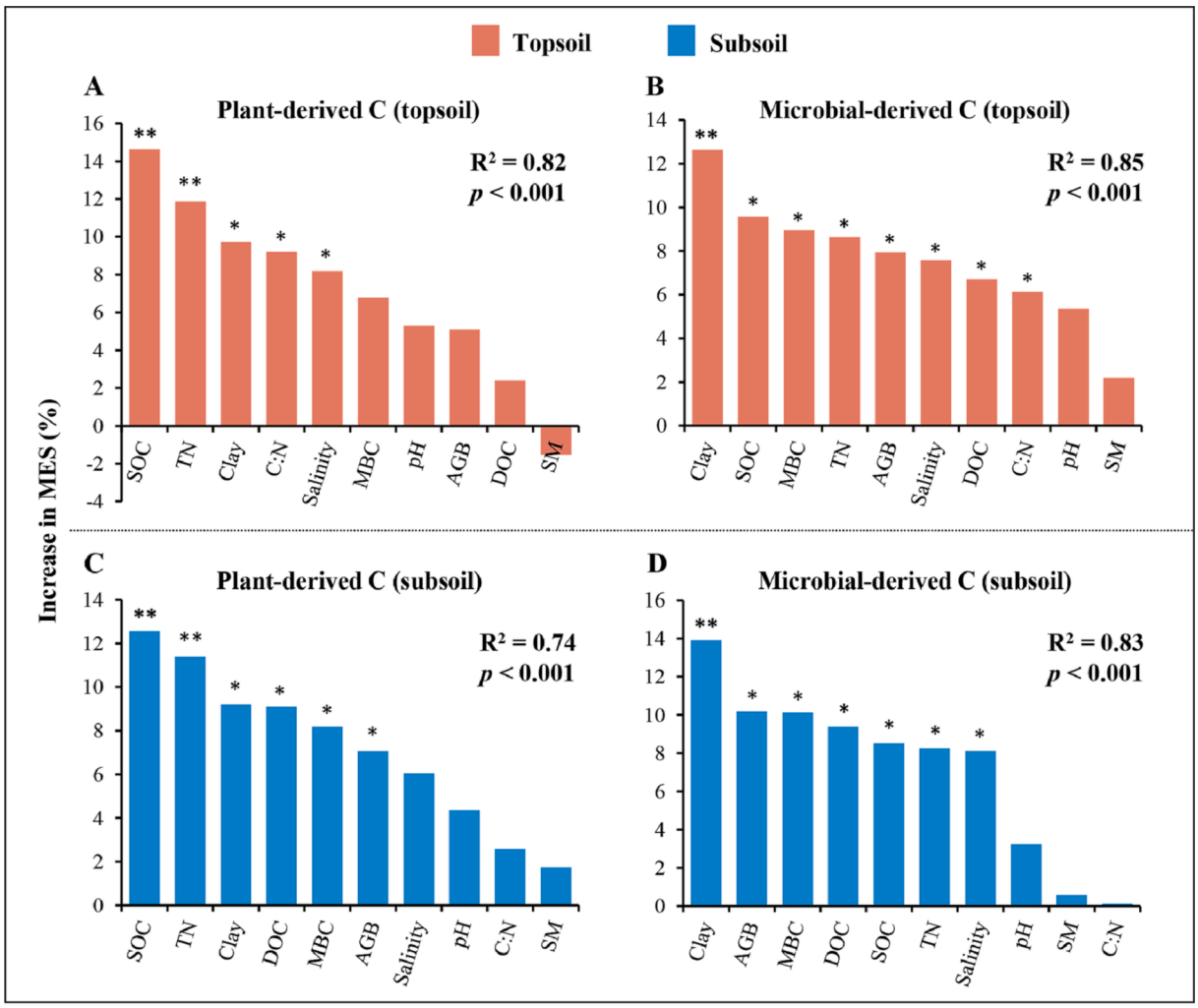

Fig. 4. Relative importance of independent variables controlling plant- and microbial-derived C in the topsoil (A and B) and subsoil (C and D) by the percentage increase of the mean squared error (MSE%) using random forests models. The following variables were included: pH; salinity; clay, grain size; SM, soil moisture; SOC, soil organic C; DOC, dissolved organic C; TN, total N; C:N, SOC:TN; MBC, microbial biomass C; and AGB, above-ground biomass. $^{*}p < 0.05$; $^{**}p < 0.01$. (For an explanation of the colour reference in this legend, please refer to the Web version of this article.).

derived C initially increased and then decreased, with the highest value occurring in the SA15 soil, consistent with changes in SOC content (Figs. 2 and 3). In contrast, microbial-derived C gradually increased with invasion time, peaking in the SA21 soil (Fig. 3). At both soil depths, a positive correlation was observed between the SOC chemical stability and the contribution of microbial-derived C to SOC ($p < 0.01$; Fig. 5). These findings emphasize the important role of microbial-derived C in SOC stability. For the plant-derived C, the increased ratios of $(Ad/Al)_v$ and $(Ad/Al)_s$ in the lignin phenols revealed increased microbial oxidation of side chains, and the decreased ratios of C/V and S/V indicated an increased microbial transformation stage (Sokol et al., 2019; Chen et al., 2021b). The SA21 soil exhibited the highest $(Ad/Al)_v$ and $(Ad/Al)_s$ ratios and the lowest ratios of C/V and S/V ratios at both soil depths across *S. alterniflora* invasion times, indicating greater decomposition of plant-derived C compared to that of the other sites (Fig. 3). For microbial-derived C, bacterial-derived C is less stable and decomposes faster than fungal-derived C (Chen et al., 2021b). The F/B ratio in both soil depths of SA21 was generally higher than that of the other sites (Fig. 3), suggesting relatively higher stability of microbial-derived C in SA21 compared to that of other sites. Therefore, considering the chemical constituents of both sources and SOC chemical stability, SA21 had lower SOC content but higher SOC stability than SA15.

Previous studies have reported that plant-derived C is mostly stored in particulate organic matter and thus is less protected than microbial-derived C; however, it can accumulate indefinitely. In contrast, microbial-derived C tends to accumulate in mineral-associated organic matter and is more stable than plant-derived C; however, it can become saturated (Angst et al., 2021; Chen et al., 2021b; Jia et al., 2021). For example, in the topsoil, the SA21 soil had 83 % higher plant AGB and 55 % higher microbial-derived C compared to the SA15 soil, while plant-derived C was 2.9 times lower in SA21 soil than in the SA15 soil (Fig. 3 and Table S1). The transition from anoxic to aerobic conditions (e.g., from SA15 in the upper part of the intertidal zone to SA21 in the supralittoral zone) reduced inundation frequency and increased oxygen exposure, thereby enhancing the growth of *S. alterniflora* and microorganisms (Fig. 6 and Table 1 and Table S1). In contrast, this transition may also cause a rapid increase in SOC mineralization (Keiluweit et al., 2017), supported by the lower C:N ($p = 0.009$), C/V ($p = 0.006$), and S/V ($p = 0.001$) ratios and higher $(Ad/Al)_v$ ($p = 0.047$) and $(Ad/Al)_s$ ($p = 0.008$) ratios in SA21 than those of SA15 in the topsoil (Fig. 3 and Table 1). Alternatively, it may promote the enrichment of microbial-derived C at the expense of plant-derived C (Liu et al., 2021a) (Figs. 3 and 6), suggesting that decreased inundation frequency can enhance the soil microbial carbon pump during *S. alterniflora* invasions. Hence, our results have vital significance for potential C loss under the long-term impacts of *S. alterniflora* invasions and indicate that these impacts

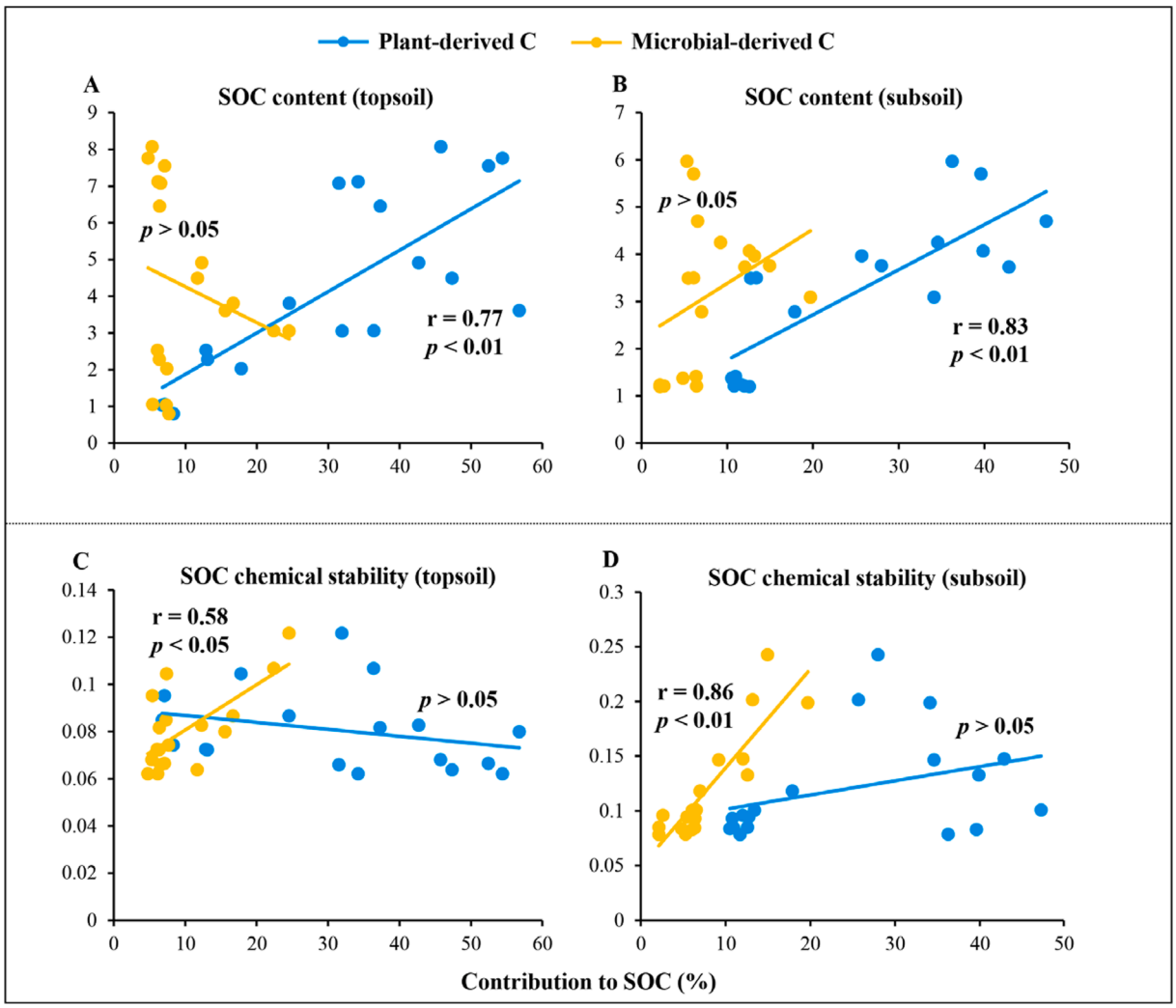

Fig. 5. Correlation of SOC content (A and B) and chemical stability (C and D) with contributions of the plant- and microbial-derived C in the topsoil and subsoil. (For an explanation of the colour reference in this legend, please refer to the Web version of this article.).

should be considered to avoid overestimating blue C pools.

The SOC content was higher in most topsoil than in the subsoil, while SOC stability was higher in the subsoil than in the topsoil (Fig. 2). This difference may be attributed to the following three reasons. First, the proliferated root system of *S. alterniflora* is mainly in the 0–30 cm surface soil layer and the impact of plant C inputs diminishes with soil depth (Yang, 2019; Yang and Chen, 2021; He et al., 2022). Second, the effect of mineral protection strengthens with soil depth (He et al., 2022). Last, the subsoil may undergo a longer period of microbial transformation compared to the topsoil (Ma et al., 2020; He et al., 2022), supported by the higher $(Ad/Al)_v$ ($p < 0.001$), $(Ad/Al)_s$ ($p < 0.001$), and F/B ratios ($p = 0.002$) in the subsoil compared to those in the topsoil (Fig. 3). Therefore, the SOC content and stability distinctly vary in the topsoil and subsoil owing to the differences in SOC sources and soil environments.

4.3. Environmental controls over SOC formation

The random forest modelling and correlation analysis revealed that plant-derived C primarily affected by SOC, TN, and clay content, whereas microbial-derived C was primarily affected by MBC, AGB, and clay content (Fig. 4 and Table 1). The important role of SOC and TN in explaining the variation of plant-derived C suggests that high soil fertility can promote an increase in plant biomass and plant C inputs into the soil. Consequently, soil fertility plays a key role in mediating the accumulation plant-derived C (Liao et al., 2021; Ding et al., 2023). Numerous studies in coastal wetlands have shown that SOC storage and stability are controlled by fine particles (Zhang et al., 2010; Xia et al., 2021). For instance, plant-derived C tends to accumulate in particulate organic matter (coarse particle) and significantly contributes to fast-cycling SOC (Zhang et al., 2010). In contrast, mineral-associated organic matter mostly residing in the fine particles, which mainly consisting of microbial-derived C, significantly contributes to slow-cycling SOC (Xia et al., 2021). In this study, both plant- and microbial-derived C were positively correlated with clay content ($p < 0.05$; Table S2); however, clay content explained a higher variation in the accumulation of microbial-derived C relative to plant-derived C (Fig. 4). This further suggests that microbial-derived C is more likely to be physically protected in mineral-associated organic matter. Previous studies have indicated a strong association between microbial-derived and MBC, suggesting that high MBC increases SOC through microbial-derived C accumulation (Shao et al., 2019a; Almagro et al., 2021). The decrease in inundation frequency and increase in oxygen exposure and plant AGB with *S. alterniflora* invasion time promote microbial growth and biomass formation, thereby increasing the quantity of microbial-derived C (Figs. 1 and 3 and Table 1 and Table S1) (Liu et al., 2021b; Yang et al., 2022). Furthermore, random forest modelling showed that salinity also influences microbial-derived C ($p < 0.05$; Fig. 4). Numerous studies have revealed that microbial biomass significantly decreases with increasing soil salinity, leading to a decline in microbial-derived C (Chen et al.,

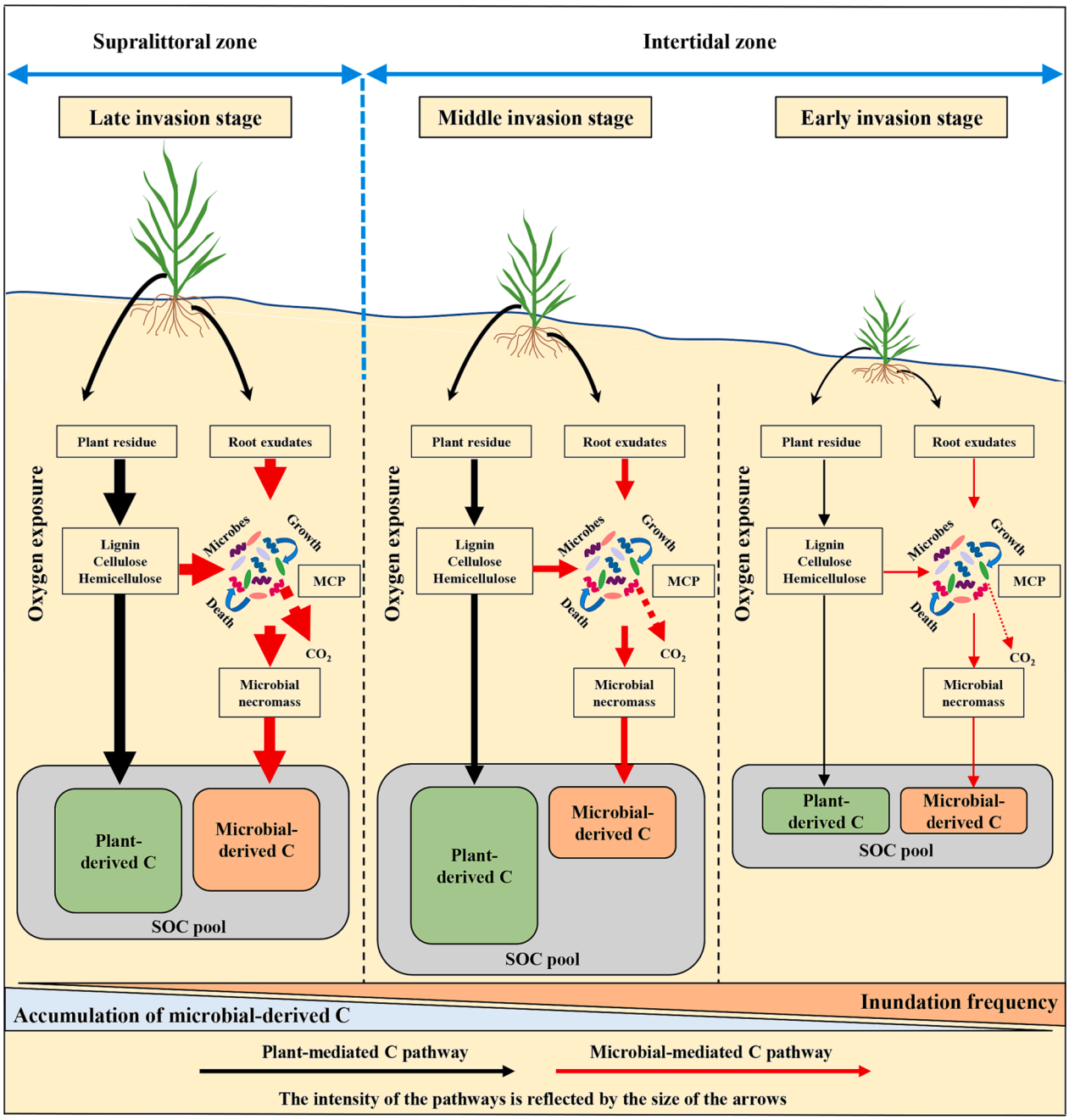

Fig. 6. Concept diagram illustrating the formation of SOC across *S. alterniflora* invasion times (early invasion stage, middle invasion stage, and late invasion stage) on the prograding coastal wetlands. The pathways of plant- and microbial-derived C are represented by black and red arrows, respectively. The intensity of the pathways is reflected by the size of the arrows. With increasing invasion time of *S. alterniflora*, the inundation frequency decreases and oxygen exposure increases. This leads to the enhancement in plant above-ground and below-ground biomass, input of root exudates, microbial respiration (CO_2 release), and soil microbial carbon pump (MCP) (Snedden et al., 2015; Davidson et al., 2018; Deng et al., 2021; Liu et al., 2021). Microbial-derived C gradually increases with increasing invasion time, whereas plant-derived C initially increases and then decreases, consistent with changes in SOC content. (For an explanation of the colour reference in this legend, please refer to the Web version of this article.). (For interpretation of the references to colour in this figure legend, the reader is referred to the web version of this article.)

2021a; Shao et al., 2022). In this study, owing to the combined influence of tidal inundation and evapotranspiration, salinity initially increased and then decreased with *S. alterniflora* invasion time and wetland elevation, instead of increasing monotonically (Fig. 1 and Table 1) (Liu et al., 2020). Therefore, SA21 had lower salinity than the other sites except BF (Table 1), but its microbial-derived C was significantly higher than that of the other sites ($p < 0.001$; Fig. 3).

Therefore, periodic tidal inundation and exposure, which are fundamental hydrological characteristics of coastal wetlands, are key factors affecting the accumulation of plant- and microbial-derived C across *S. alterniflora* invasion times (Zhu et al., 2019; Hill and Vargas, 2022). Considering the spatio-temporal variability of hydrological conditions in coastal wetlands and the complex interactions with other factors, such as plant biological traits, topography, and edaphic variables, long-term positioning observations at more sites should be performed to fully understand the long-term invasion impacts of *S. alterniflora* on C burial. Furthermore, it is essential to uncover the underlying mechanisms in the context of climate change and sea level

rise and develop a model depicting the dynamics of *S. alterniflora* salt marsh ecosystem characterized by coupled environmental–ecological processes (Wang et al., 2012; Schuerch et al., 2019).

5. Conclusion

Our study suggests that plant-derived C dominated in SOC content compared to microbial-derived C during *S. alterniflora* invasions, while microbial-derived C played a more crucial role in SOC stability than that of plant-derived C. We observed a gradual increase in microbial-derived C with invasion time at both soil depths, whereas plant-derived C initially increased and then decreased, consistent with changes in SOC content. The variation in inundation conditions under tidal action emerged as a crucial factor affecting the accumulation of plant- and microbial-derived C and the SOC stability. Decreased inundation frequency and increased oxygen exposure driven by tides may accelerate SOC mineralization and enhance the enrichment of microbial-derived C at the expense of plant-derived C, thereby improving SOC stability. Consequently, this study has vital implications for understanding potential C loss in terms of the long-term impacts of *S. alterniflora* invasions. Furthermore, it facilitates the prediction of long-term effects of *S. alterniflora* invasions on blue C budgets under global change scenarios.

CRediT authorship contribution statement

Qihang Liao: Conceptualization, Data curation, Formal analysis, Investigation, Methodology, Visualization, Writing – original draft, Writing – review & editing. **Feng Yuan:** Conceptualization, Data curation, Writing – review & editing. **Qinya Fan:** Formal analysis, Investigation, Methodology, Writing – review & editing. **Hongyu Chen:** Conceptualization, Software, Supervision, Writing – review & editing. **Yameng Wang:** Formal analysis, Methodology, Resources. **Chuchu Zhang:** Data curation, Validation, Visualization. **Chao Lu:** Conceptualization, Writing – original draft. **Penghua Qiu:** Funding acquisition, Project administration, Resources, Supervision. **Chenglong Wang:** Conceptualization, Funding acquisition, Supervision, Validation, Visualization, Writing – original draft, Writing – review & editing. **Xinqing Zou:** Conceptualization, Funding acquisition, Supervision, Validation, Writing – original draft, Writing – review & editing.

Declaration of competing interest

The authors declare that they have no known competing financial interests or personal relationships that could have appeared to influence the work reported in this paper.

Data availability

Data will be made available on request.

Acknowledgements

This work received support from the Natural Science Foundation of China (grant number 42106056), the Fundamental Research Funds for the Central Universities (grant number 0209-14370407), the Innovation Platform for Academicians of Hainan Province and its specific research fund (grant number YSPTZX202128), and the Innovation Project of Marine Science and Technology of Jiangsu Province (grant number JSZRHYKJ202206).

Appendix A. Supplementary data

Supplementary data to this article can be found online at https://doi.org/10.1016/j.catena.2023.107777.

References

Almagro, M., Ruiz-Navarro, A., Díaz-Pereira, E., Albaladejo, J., Martínez-Mena, M., 2021. Plant residue chemical quality modulates the soil microbial response related to decomposition and soil organic carbon and nitrogen stabilization in a rainfed Mediterranean agroecosystem. Soil Biol. Biochem. 156, 108198 https://doi.org/10.1016/j.soilbio.2021.108198.

Angst, G., Mueller, K.E., Nierop, K.G.J., Simpson, M.J., 2021. Plant- or microbial-derived? A review on the molecular composition of stabilized soil organic matter. Soil Biol. Biochem. 156, 108189 https://doi.org/10.1016/j.soilbio.2021.108189.

Bernal, B., Mitsch, W.J., 2008. A comparison of soil carbon pools and profiles in wetlands in costa rica and ohio. Ecol. Eng. 34, 311–323. https://doi.org/10.1016/j.ecoleng.2008.09.005.

Bernik, B.M., Li, H., Blum, M.J., 2016. Genetic variation of *Spartina alterniflora* intentionally introduced to china. Biol. Invasions. 18, 1485–1498. https://doi.org/10.1007/s10530-016-1096-3.

Brookes, P.C., Landman, A., Pruden, G., Jenkinson, D.S., 1985. Chloroform fumigation and the release of soil nitrogen: A rapid direct extraction method to measure microbial biomass nitrogen in soil. Soil Biol. Biochem. 17, 837–842. https://doi.org/10.1016/0038-0717(85)90144-0.

Cahoon, D.R., McKee, K.L., Morris, J.T., 2021. How plants influence resilience of salt marsh and mangrove wetlands to sea-level rise. Estuar. Coasts 44, 883–898. https://doi.org/10.1007/s12237-020-00834-w.

Calderón, F., Haddix, M., Conant, R., Magrini-Bair, K., Paul, E., 2013. Diffuse-reflectance fourier-transform mid-infrared spectroscopy as a method of characterizing changes in soil organic matter. Soil Sci. Soc. Am. J. 77, 1591–1600. https://doi.org/10.2136/sssaj2013.04.0131.

Chen, X., Hu, Y., Xia, Y., Zheng, S., Ma, C., Rui, Y., He, H., Huang, D., Zhang, Z., Ge, T., Wu, J., Guggenberger, G., Kuzyakov, Y., Su, Y., 2021b. Contrasting pathways of carbon sequestration in paddy and upland soils. Glob. Chang. Biol. 27, 2478–2490. https://doi.org/10.1111/gcb.15595.

Chen, J., Wang, H., Hu, G., Li, X., Dong, Y., Zhuge, Y., He, H., Zhang, X., 2021a. Distinct accumulation of bacterial and fungal residues along a salinity gradient in coastal salt-affected soils. Soil Biol. Biochem. 158, 108266 https://doi.org/10.1016/j.soilbio.2021.108266.

Davidson, I.C., Cott, G.M., Devaney, J.L., Simkanin, C., 2018. Differential effects of biological invasions on coastal blue carbon: A global review and meta-analysis. Glob. Chang. Biol. 24, 5218–5230. https://doi.org/10.1111/gcb.14426.

Deng, Z., An, S., Zhou, C., Wang, Z., Zhi, Y., Wang, Y., Shi, S., Chen, L., Zhao, C., 2007. Genetic structure and habitat selection of the tall form *Spartina alterniflora* Loisel. in china. Hydrobiologia. 583, 195–204. https://doi.org/10.1007/s10750-006-0529-x.

Ding, X., Wang, W., Wen, J., Feng, T., Peñuelas, J., Sardans, J., Liang, C., Agathokleous, E., Wang, C., Song, Z., Li, Q., Filley, T.R., He, H., Zhang, X., 2023. *Spartina alterniflora* invasion differentially alters microbial residues and their contribution to soil organic C in coastal marsh and mangrove wetlands. Catena. 230, 107246 https://doi.org/10.1016/j.catena.2023.107246.

Ge, Z.M., Li, S.H., Tan, L.S., Li, Y.L., Hu, Z.J., 2019. The importance of the propagule-sediment-tide "power balance" for revegetation at the coastal frontier. Ecol. Appl. 29, e1967.

He, M., Fang, K., Chen, L., Feng, X., Qin, S., Kou, D., He, H., Liang, C., Yang, Y., 2022. Depth-dependent drivers of soil microbial necromass carbon across tibetan alpine grasslands. Glob. Chang. Biol. 28, 936–949. https://doi.org/10.1111/gcb.15969.

Hill, A.C., Vargas, R., 2022. Methane and carbon dioxide fluxes in a temperate tidal salt marsh: Comparisons between plot and ecosystem measurements. Journal of geophysical research Biogeosciences. 127 https://doi.org/10.1029/2022JG006943 e2022JG006943.

Hopkinson, C.S., Cai, W., Hu, X., 2012. Carbon sequestration in wetland dominated coastal systems - A global sink of rapidly diminishing magnitude. Curr. Opin. Environ. Sustain. 4, 186–194. https://doi.org/10.1046/j.0022-0477.2001.00632.x.

Hou, Y., Chen, Y., Chen, X., He, K., Zhu, B., 2019. Changes in soil organic matter stability with depth in two alpine ecosystems on the tibetan plateau. Geoderma 351, 153–162. https://doi.org/10.1016/j.geoderma.2019.05.034.

Indorf, C., Dyckmans, J., Khan, K.S., Joergensen, R.G., 2011. Optimisation of amino sugar quantification by HPLC in soil and plant hydrolysates. Biol. Fertil. Soils 47, 387–396. https://doi.org/10.1007/s00374-011-0545-5.

Y. Jia G. Zhai S. Zhu X. Liu B. Schmid Z. Wang K. Ma X. Feng Plant and microbial pathways driving plant diversity effects on soil carbon accumulation in subtropical forest Soil Biol. Biochem. 161 2021 108375 10.1016/j.soilbio.2021.108375.

Jiao, N., Zheng, Q., 2011. The microbial carbon pump: from genes to ecosystems. Appl. Environ. Microbiol. 77, 7439–7444. https://doi.org/10.1128/AEM.05640-11.

Jin, B., Lai, D.Y.F., Gao, D., Tong, C., Zeng, C., 2017. Changes in soil organic carbon dynamics in a native C_4 plant-dominated tidal marsh following *Spartina alterniflora* invasion. Pedosphere. 27, 856–867. https://doi.org/10.1016/S1002-0160(17)60396-5.

Keiluweit, M., Wanzek, T., Kleber, M., Nico, P., Fendorf, S., 2017. Anaerobic microsites have an unaccounted role in soil carbon stabilization. Nat. Commun. 8, 1771. https://doi.org/10.1038/s41467-017-01406-6.

Kögel, I., 1986. Estimation and decomposition pattern of the lignin component in forest humus layers. Soil Biol. Biochem. 18, 589–594. https://doi.org/10.1016/0038-0717(86)90080-5.

Li, N., Li, B., Nie, M., Wu, J., 2020. Effects of exotic *Spartina alterniflora* on saltmarsh nitrogen removal in the Yangtze River Estuary China. J. Clea. Prod. 271, 122557 https://doi.org/10.1016/j.jclepro.2020.122557.

Liang, C., Schimel, J.P., Jastrow, J.D., 2017. The importance of anabolism in microbial control over soil carbon storage. Nat. Microbiol. 2, 17105. https://doi.org/10.1038/nmicrobiol.2017.105.

Liang, C., Amelung, W., Lehmann, J., Kästner, M., 2019. Quantitative assessment of microbial necromass contribution to soil organic matter. Glob. Chang. Biol. 25, 3578–3590. https://doi.org/10.1111/gcb.14781.
Liao, Q., Liu, H., Lu, C., Liu, J., Waigi, M.G., Ling, W., 2021. Root exudates enhance the PAH degradation and degrading gene abundance in soils. Sci. Total Environ. 764, 144436 https://doi.org/10.1016/j.scitotenv.2020.144436.
Liao, Q., Lu, C., Yuan, F., Fan, Q., Chen, H., Yang, L., Qiu, P., Feng, Z., Wang, C., Zou, X., 2023. Soil carbon-fixing bacterial communities respond to plant community change in coastal salt marsh wetlands. Appl. Soil Ecol. 189, 104918 https://doi.org/10.1016/j.apsoil.2023.104918.
Liu, W., Chen, X., Strong, D.R., Pennings, S.C., Kirwan, M.L., Chen, X., Zhang, Y., 2020. Climate and geographic adaptation drive latitudinal clines in biomass of a widespread saltmarsh plant in its native and introduced ranges. Limnol. Oceanogr. 65, 1399–1409. https://doi.org/10.1002/lno.11395.
Liu, J., Han, R., Su, H., Wu, Y., Zhang, L., Richardson, C.J., Wang, G., 2017. Effects of exotic *Spartina alterniflora* on vertical soil organic carbon distribution and storage amount in coastal salt marshes in Jiangsu, China. Ecol. Eng. 106, 132–139. https://doi.org/10.1016/j.ecoleng.2017.05.041.
Liu, C., Wang, S., Zhu, E., Jia, J., Zhao, Y., Feng, X., 2021a. Long-term drainage induces divergent changes of soil organic carbon contents but enhances microbial carbon accumulation in fen and bog. Geoderma. 404, 115343 https://doi.org/10.1016/j.geoderma.2021.115343.
Liu, H., Xu, X., Zhou, C., Zhao, J., Li, B., Nie, M., 2021b. Geographic linkages of root traits to salt marsh productivity. Ecosyst. 24, 726–737. https://doi.org/10.1007/s10021-020-00546-z.
Ma, T., Zhu, S., Wang, Z., Chen, D., Dai, G., Feng, B., Su, X., Hu, H., Li, K., Han, W., Liang, C., Bai, Y., Feng, X., 2018. Divergent accumulation of microbial necromass and plant lignin components in grassland soils. Nat. Commun. 9, 3480. https://doi.org/10.1038/s41467-018-05891-1.
Ma, T., Dai, G., Zhu, S., Chen, D., Chen, L., Lü, X., Wang, X., Zhu, J., Zhang, Y., He, J., Bai, Y., Han, X., Feng, X., 2020. Vertical variations in plant- and microbial-derived carbon components in grassland soils. Plant and Soil 446, 441–455. https://doi.org/10.1007/s11104-019-04371-9.
Margenot, A.J., Hodson, A.K., 2016. Relationships between labile soil organic matter and nematode communities in a california oak woodland. Nematol. 18, 1231–1245. https://doi.org/10.1163/15685411-00003027.
Otto, A., Shunthirasingham, C., Simpson, M.J., 2005. A comparison of plant and microbial biomarkers in grassland soils from the Prairie Ecozone of Canada. Org Geochem. 36, 425–448. https://doi.org/10.1016/j.orggeochem.2004.09.008.
Ouyang, X., Lee, S.Y., 2014. Updated estimates of carbon accumulation rates in coastal marsh sediments. Biogeosciences. 11, 5057–5071. https://doi.org/10.5194/bg-11-5057-2014.
Ouyang, X., Lee, S.Y., Connolly, R.M., 2017. The role of root decomposition in global mangrove and saltmarsh carbon budgets. Earth Sci. Rev. 166, 53–63. https://doi.org/10.1016/j.earscirev.2017.01.004.
Ryzak, M., Bieganowski, A., 2011. Methodological aspects of determining soil particle-size distribution using the laser diffraction method. J. Plant Nutr. Soil Sci. 174, 624–633. https://doi.org/10.1002/jpln.2010002.
Schuerch, M., Spencer, T., Evans, B., 2019. Coupling between tidal mudflats and salt marshes affects marsh morphology. Mar. Geol. 412, 95–106. https://doi.org/10.1016/j.margeo.2019.03.008.
Seliskar, D.M., Gallagher, J.L., Burdick, D.M., Mutz, L.A., 2002. The regulation of ecosystem functions by ecotypic variation in the dominant plant: A *Spartina alterniflora* salt-marsh case study. The J. Ecol. 90, 1–11. https://doi.org/10.1046/j.0022-0477.2001.00632.x.
Shao, P., Liang, C., Lynch, L., Xie, H., Bao, X., 2019a. Reforestation accelerates soil organic carbon accumulation: Evidence from microbial biomarkers. Soil Biol. Biochem. 131, 182–190. https://doi.org/10.1016/j.soilbio.2019.01.012.
Shao, P., Liang, C., Rubert-Nason, K., Li, X., Xie, H., Bao, X., 2019b. Secondary successional forests undergo tightly-coupled changes in soil microbial community structure and soil organic matter. Soil Biol. Biochem. 128, 56–65. https://doi.org/10.1016/j.soilbio.2018.10.004.
Shao, P., Han, H., Sun, J., Yang, H., Xie, H., 2022. Salinity effects on microbial derived-C of coastal wetland soils in the Yellow River delta. Front. Ecol. Evol. 10 https://doi.org/10.3389/fevo.2022.87281.
Snedden, G.A., Cretini, K., Patton, B., 2015. Inundation and salinity impacts to above- and belowground productivity in *Spartina patens* and *Spartina alterniflora* in the Mississippi River deltaic plain: Implications for using river diversions as restoration tools. Ecol. Eng. 81, 133–139. https://doi.org/10.1016/j.ecoleng.2015.04.035.
Sokol, N.W., Sanderman, J., Bradford, M.A., 2019. Pathways of mineral-associated soil organic matter formation: Integrating the role of plant carbon source, chemistry, and point of entry. Glob. Chang. Biol. 25, 12–24. https://doi.org/10.1111/gcb.14482.
Spivak, A.C., Sanderman, J., Bowen, J.L., Canuel, E.A., Hopkinson, C.S., 2019. Global-change controls on soil-carbon accumulation and loss in coastal vegetated ecosystems. Nat. Geosci. 12, 685–692. https://doi.org/10.1038/s41561-019-0435-2.
Viles, H., 2020. Biogeomorphology: Past, present and future. Geomorphology 366, 106809. https://doi.org/10.1016/j.geomorph.2019.06.022.
Wan, S., Qin, P., Liu, J., Zhou, H., 2009. The positive and negative effects of exotic *Spartina alterniflora* in China. Ecol. Eng. 35, 444–452. https://doi.org/10.1016/j.ecoleng.2008.05.020.
B. Wang K. Zhang Q.X. Liu Q. He J. van de Koppel S.N. Teng X. Miao M. Liu M.D. Bertness C. Xu, 2022. Long-distance facilitation of coastal ecosystem structure and resilience. Proceedings of the National Academy of Sciences of the United States of America 119, e2123274119. https://doi.org/10.1073/pnas.2123274119.
Wang, Y.P., Gao, S., Jia, J., Thompson, C.E.L., Gao, J., Yang, Y., 2012. Sediment transport over an accretional intertidal flat with influences of reclamation, Jiangsu coast, China. Mar. Geol. 291–294, 147–161. https://doi.org/10.1016/j.margeo.2011.01.004.
Wang, F., Sanders, C.J., Santos, I.R., Tang, J., Schuerch, M., Kirwan, M.L., Kopp, R.E., Zhu, K., Li, X., Yuan, J., Liu, W., Li, Z., Naturvetenskapliga, F., Faculty, O.S., Göteborgs, U., Gothenburg, U., Institutionen, F.M.V., 2021. Global blue carbon accumulation in tidal wetlands increases with climate change. National Science Review 8 nwaa296. https://doi.org/10.1093/nsr/nwaa296.
Xia, S., Wang, W., Song, Z., Kuzyakov, Y., Guo, L., Van Zwieten, L., Li, Q., Hartley, I.P., Yang, Y., Wang, Y., Andrew Quine, T., Liu, C., Wang, H., 2021. *Spartina alterniflora* invasion controls organic carbon stocks in coastal marsh and mangrove soils across tropics and subtropics. Glob. Chang. Biol. 27, 1627–1644. https://doi.org/10.1111/gcb.15516.
Xiang, J., Liu, D., Ding, W., Yuan, J., Lin, Y., 2015. Invasion chronosequence of *Spartina alterniflora* on methane emission and organic carbon sequestration in a coastal salt marsh. Atmos. Environ. 112, 72–80. https://doi.org/10.1016/j.atmosenv.2015.04.035.
Xie, W., Gao, S., 2013. Invasive *Spartina alterniflora*-induced factors affecting epibenthos distribution in coastal salt marsh, China. Acta Oceanol. Sin. 32, 81–88. https://doi.org/10.1007/s13131-013-0280-x.
Xu, X., Wei, S., Chen, H., Li, B., Nie, M., 2022. Effects of *Spartina* invasion on the soil organic carbon content in salt marsh and mangrove ecosystems in China. J. Appl. Ecol. 59, 1937–1946. https://doi.org/10.1111/1365-2664.14202.
Yang, R.M., 2019. Interacting effects of plant invasion, climate, and soils on soil organic carbon storage in coastal wetlands. J. Geophys. Res. Biogeo. 124, 2554–2564. https://doi.org/10.1029/2019JG005190.
Yang, W., An, S., Zhao, H., Xu, L., Qiao, Y., Cheng, X., 2016. Impacts of *Spartina alterniflora* invasion on soil organic carbon and nitrogen pools sizes, stability, and turnover in a coastal salt marsh of eastern China. Ecol. Eng. 86, 174–182. https://doi.org/10.1016/j.ecoleng.2015.11.010.
Yang, R.M., Chen, L.M., 2021. *Spartina alterniflora* invasion alters soil bulk density in coastal wetlands of China. Land Degrad. Dev. 32, 1993–1999. https://doi.org/10.1002/ldr.3859.
Yang, Y., Dou, Y., Wang, B., Wang, Y., Liang, C., An, S., Soromotin, A., Kuzyakov, Y., 2022. Increasing contribution of microbial residues to soil organic carbon in grassland restoration chronosequence. Soil Biol. Biochem. 170, 108688 https://doi.org/10.1016/j.soilbio.2022.108688.
Yang, R., Guo, W., 2018. Exotic *Spartina alterniflora* enhances the soil functions of a coastal ecosystem. Soil Sci. Soc. Am. J. 82, 901–909. https://doi.org/10.2136/sssaj2017.12.0411.
Yuan, J., Ding, W., Liu, D., Xiang, J., Lin, Y., 2014. Methane production potential and methanogenic archaea community dynamics along the *Spartina alterniflora* invasion chronosequence in a coastal salt marsh. Appl. Microbiol. Biotechnol. 98, 1817–1829. https://doi.org/10.1007/s00253-013-5104-6.
Zhang, Y., Ding, W., Luo, J., Donnison, A., 2010. Changes in soil organic carbon dynamics in an eastern chinese coastal wetland following invasion by a C_4 plant *Spartina alterniflora*. Soil Biol. Biochem. 42, 1712–1720. https://doi.org/10.1016/j.soilbio.2010.06.006.
Zhang, X., Zhang, Z., Li, Z., Li, M., Wu, H., Jiang, M., 2021. Impacts of *Spartina alterniflora* invasion on soil carbon contents and stability in the yellow river deltachina. Sci. Total Environ. 775, 145188 https://doi.org/10.1016/j.scitotenv.2021.145188.
Zhu, X., Meng, L., Zhang, Y., Weng, Q., Morris, J., 2019. Tidal and meteorological influences on the growth of invasive *Spartina alterniflora*: Evidence from UAV remote sensing. Remote Sens. (Basel) 11, 1208. https://doi.org/10.3390/rs11101208.